Electronic Supporting Information for

Enhancement of photocatalytic H_2 production by metal complex electrostatic adsorption on TiO_2 (B) nanosheets

Xiangchen Kong, [a] Zhonghui Gao,*[b] Yue Gong,[a] Huiming Huang,[a] Haifeng Wang,[b] Porun Liu,[c] Huajie Yin,[c] Zhenduo Cui,[a] Zhaoyang Li,[a] Yanqin Liang,[a] Shengli Zhu,*[a] Yunhui Huang *[b] and Xianjin Yang [a]

[a.] *School of Materials Science and Engineering, Tianjin University, Tianjin 300350, China.*

[b.] *School of Materials Science and Engineering, Tongji University, Shanghai 201804, China.*

[c.] *Centre for Clean Environment and Energy, Gold Coast Campus, Griffith University, Queensland 4222, Australia.*

Corresponding Author

*SLZ: slzhu@tju.edu.cn

*ZHG: gzhh05080201@163.com

*YHH: huangyh@tongji.edu.cn

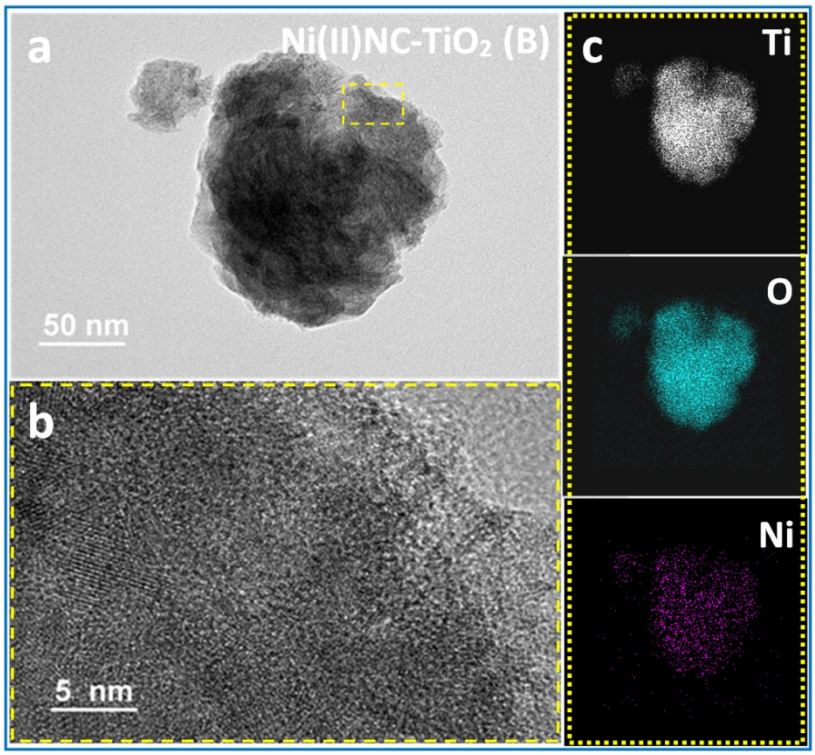

Figure S1. Structure characterizations of as-synthesized Ni(II)NC-TiO_2 (B) nanosheets. (a-b) TEM, HRTEM images of Ni(II)NC-TiO_2 (B); (c) the overlay mapping elements of Ti, O and Ni.

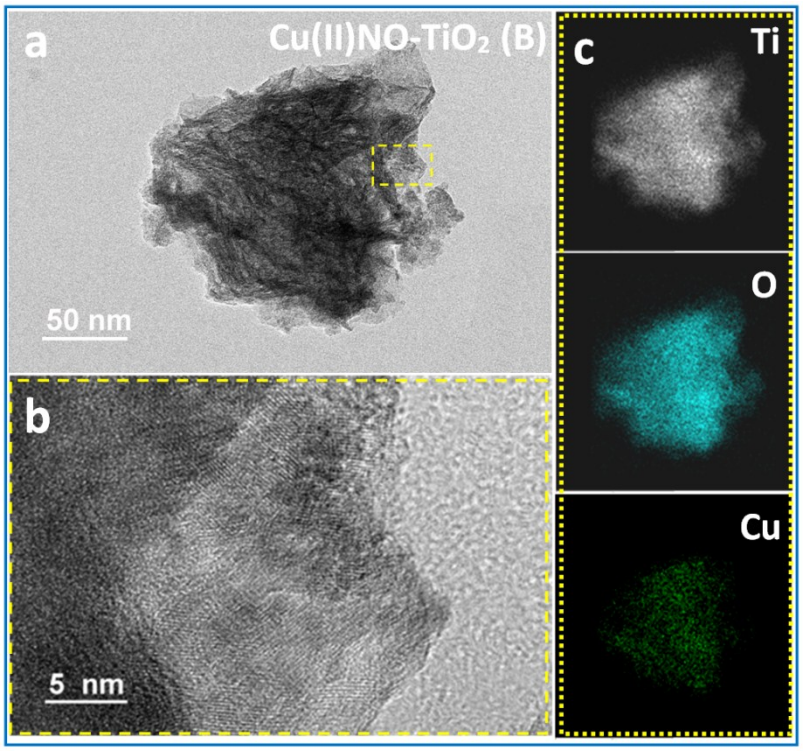

Figure S2. Structure characterizations of as-synthesized Cu(II)NO-TiO_2 (B) nanosheets. (a-b) TEM, HRTEM images of Cu(II)NO-TiO_2 (B); (c) the overlay mapping elements of Ti, O and Cu.

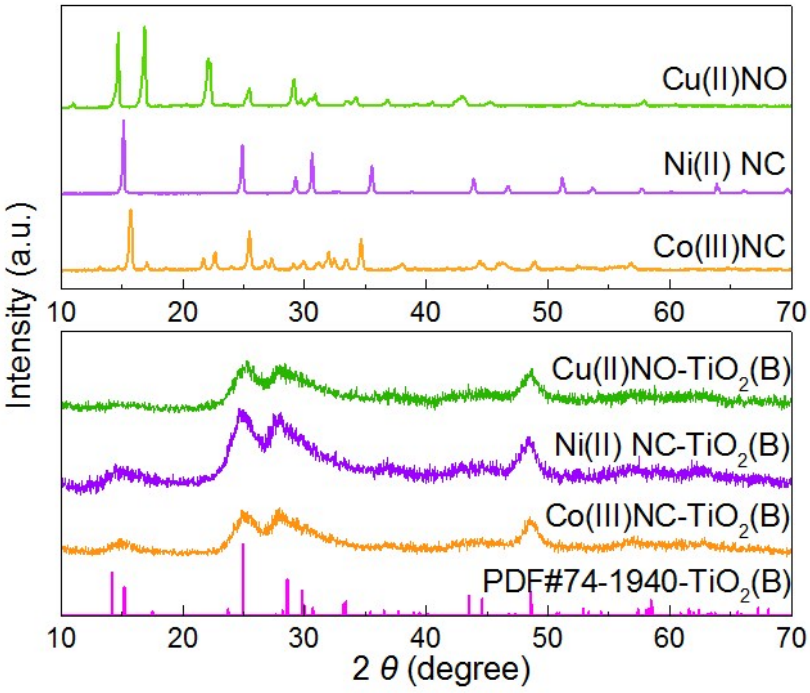

Figure S3. XRD patterns of the Co(Ⅲ)NC, Ni(II)NC and Cu(II)NO metal complexes, and Co(Ⅲ)NC/Ni(II)NC/Cu(II)NO-TiO_2 (B) nanosheets by electrostatic adsorption.

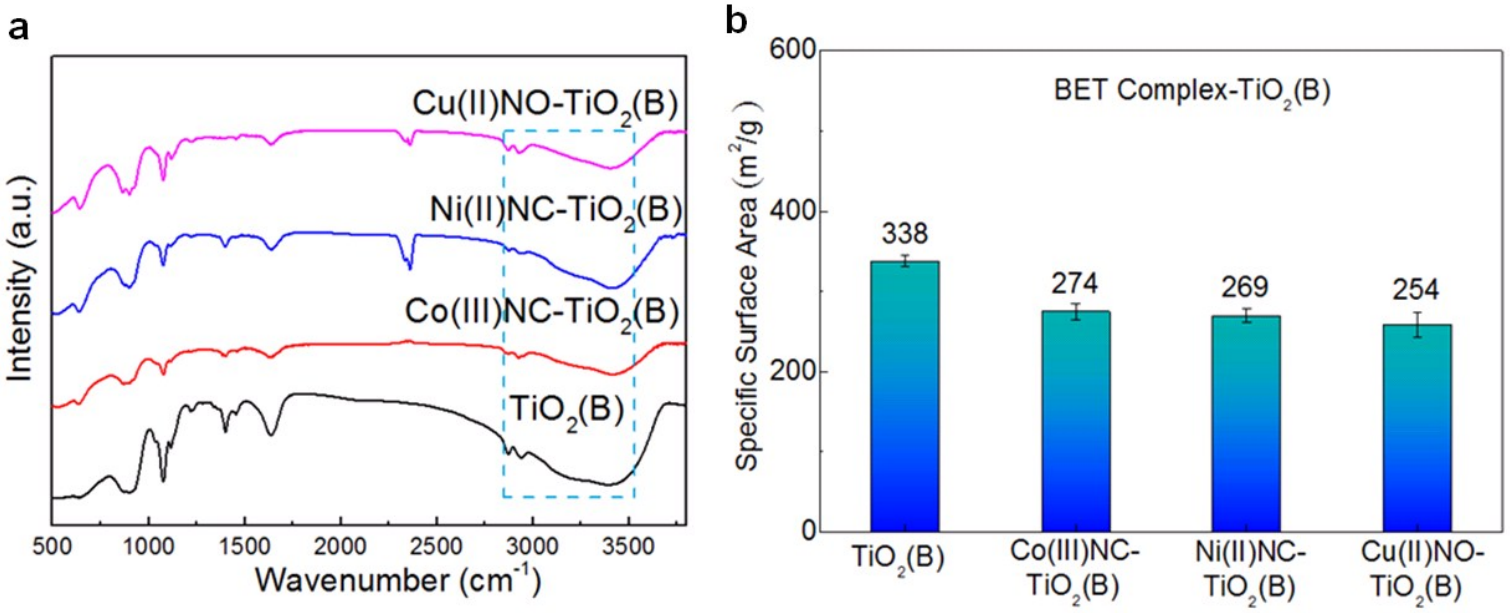

Figure S4.(a) FTIR and (b) BET of the pristine TiO_2 (B) and Co(Ⅲ)NC/Ni(II)NC/Cu(II)NO-TiO_2 (B) nanosheets by electrostatic adsorption.

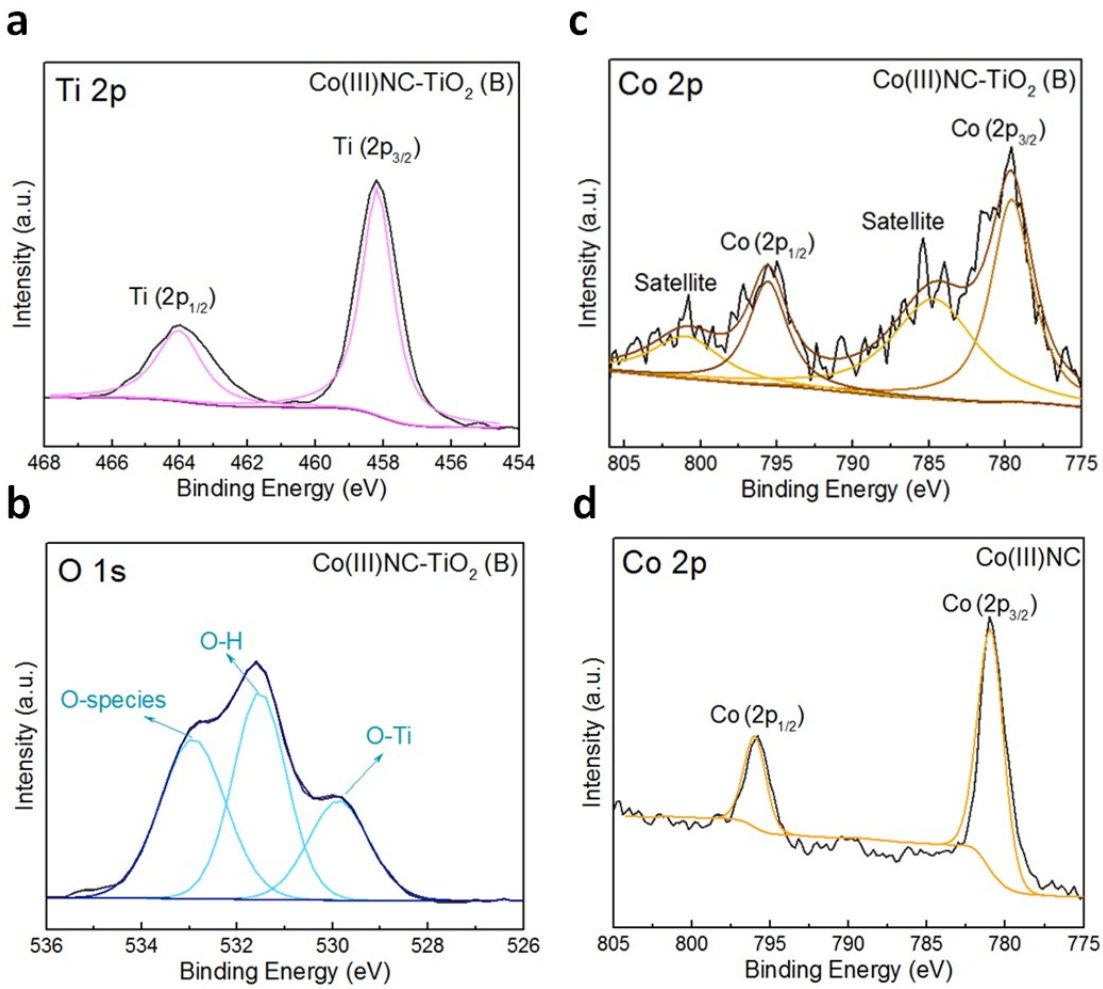

Figure S5. XPS spectra of (a) Ti 2p, (b) O 1s and (c) Co 2p region of Co(II)NC-TiO_2 (B); (d) Co 2p spectra of pristine Co(II)NC.

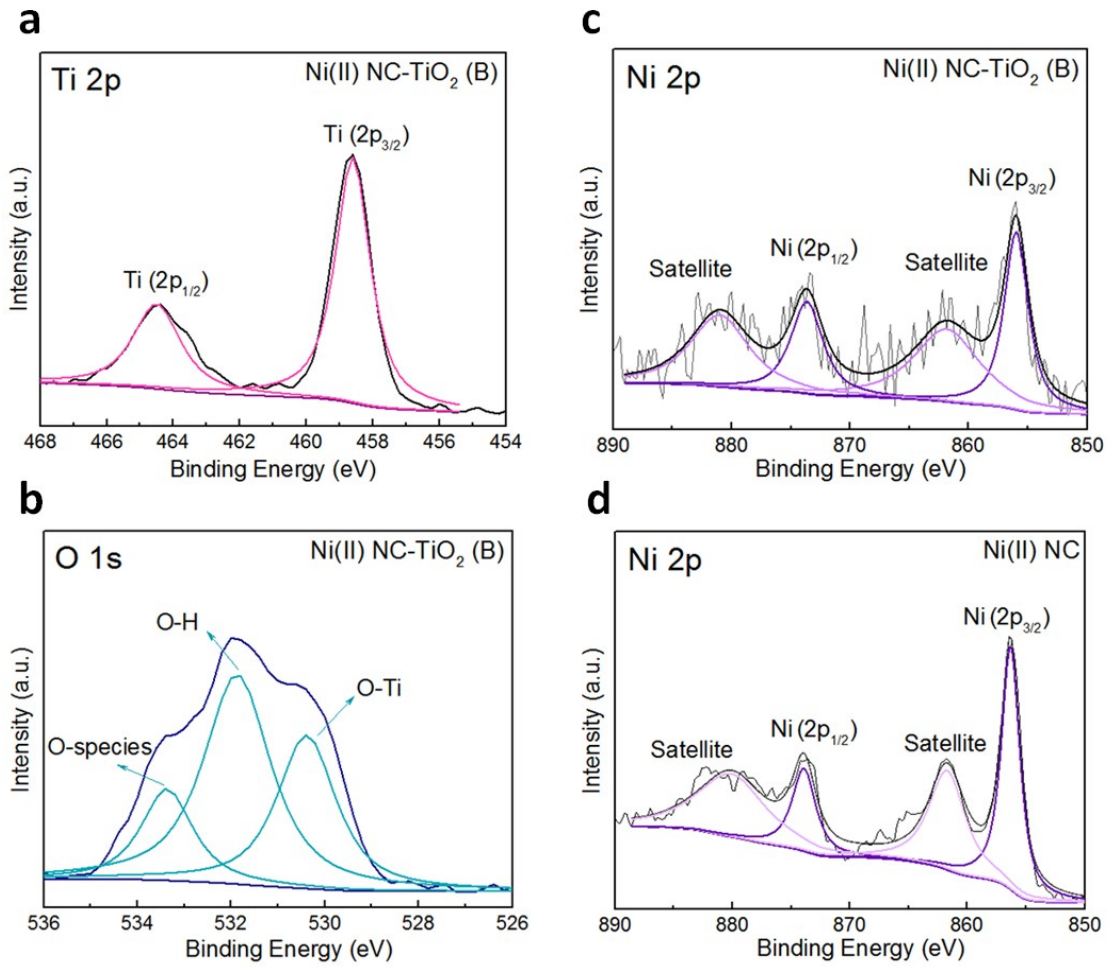

Figure S6. XPS spectra of (a) Ti 2p, (b) O 1s and (c) Ni 2p region of Ni(II)NC-TiO_2 (B); (d) Ni 2p spectra of pristine Ni(II)NC.

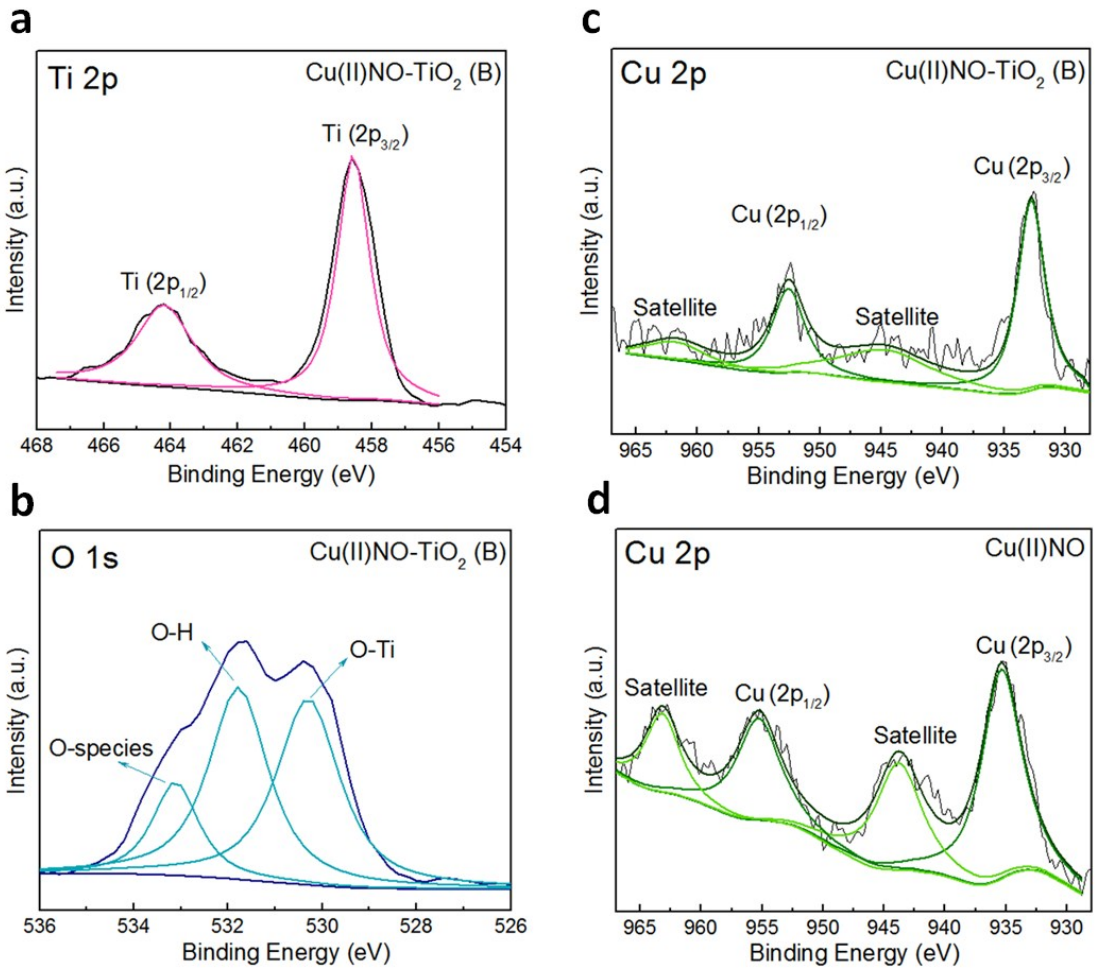

Figure S7. XPS spectra of (a) Ti 2p, (b) O 1s and (c) Cu 2p region of Cu(II)NO-TiO_2 (B); (d) Cu 2p spectra of pristine Cu(II)NO.

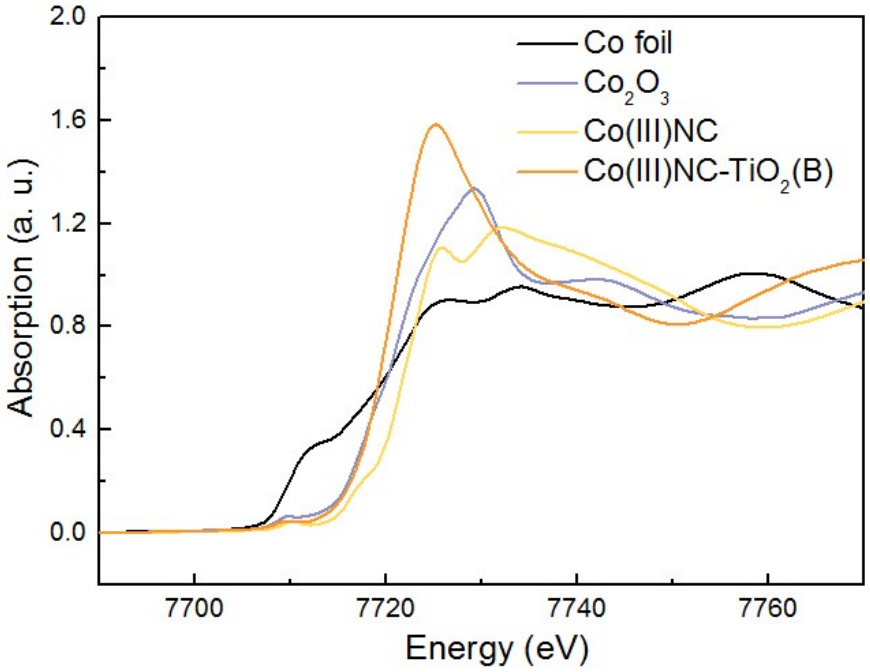

Figure S8. The overall profile of Co K-edge XANES spectra of Co(Ⅲ)NC and Co(Ⅲ)NC-TiO_2 (B) indicated the presence of trivalent Co.

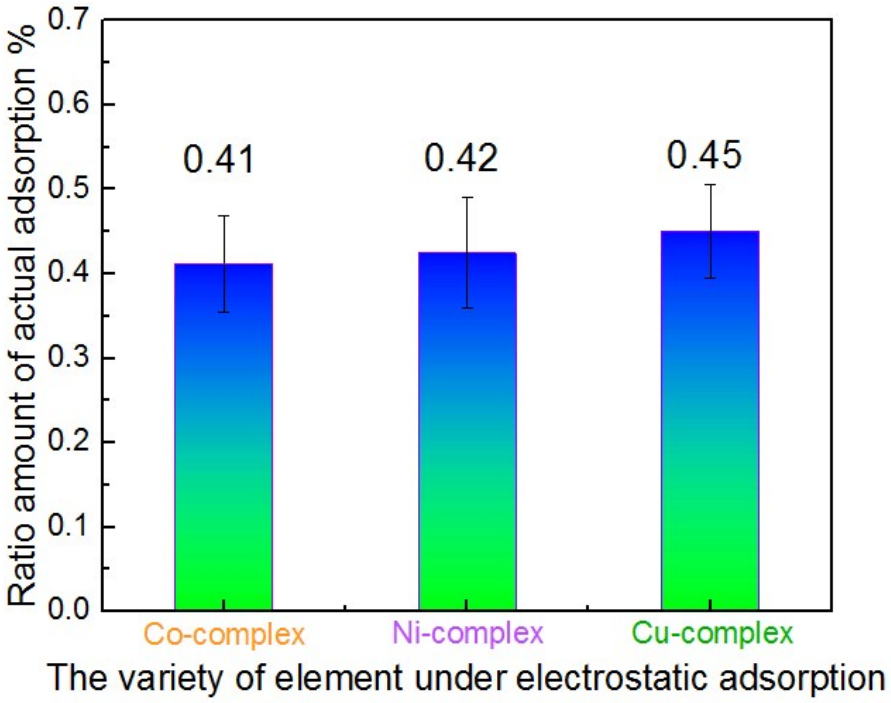

Figure S9. The actual adsorption ratio amounts of Co, Ni and Cu on TiO_2 (B) tested by ICP-OES.

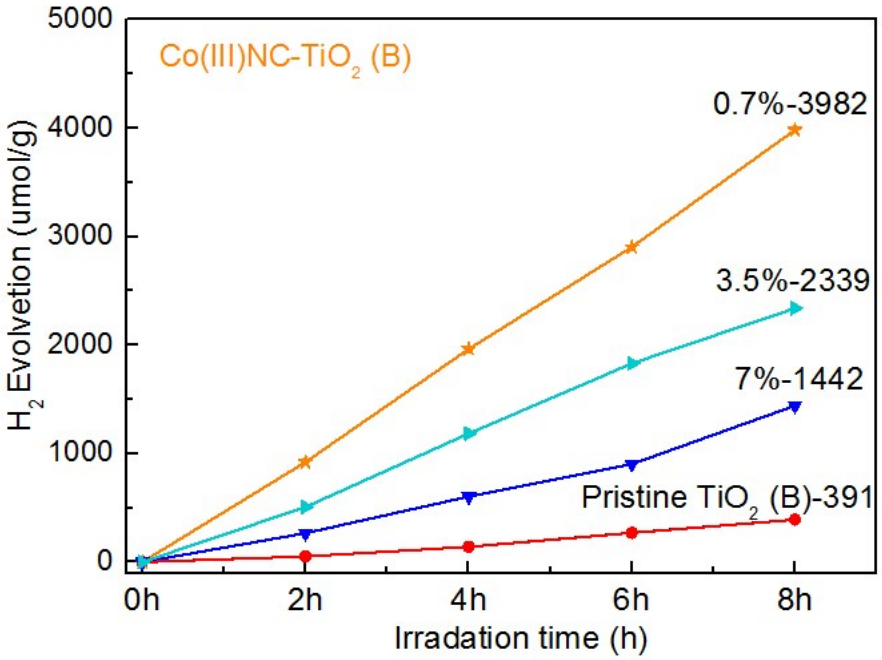

Figure S10. Photocatalytic H_2 evolution activities of Co(III)NC-TiO_2 (B) with different loading contents.

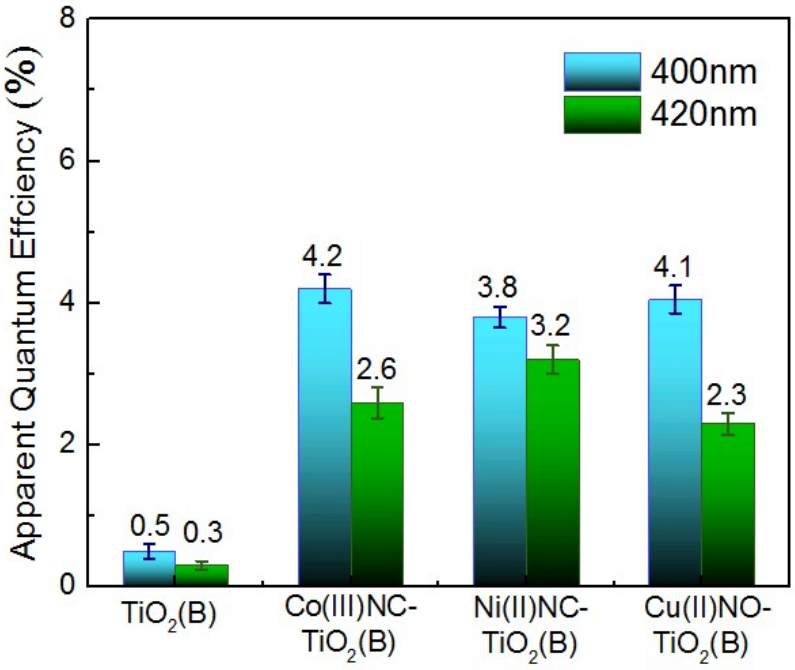

Figure S11. AQE of pristine TiO_2 (B), Co(III)NC-TiO_2 (B), Ni(II)NC-TiO_2 (B) and Cu(II)NO-TiO_2 (B) nanosheets at 400nm and 420nm.

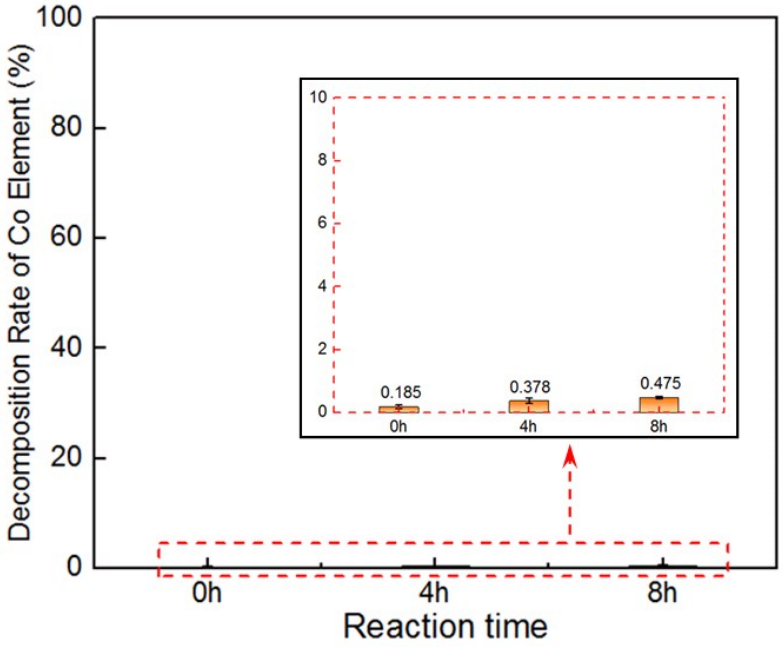

Figure S12. the decomposition rate of Co element with different photocatalytic reaction time

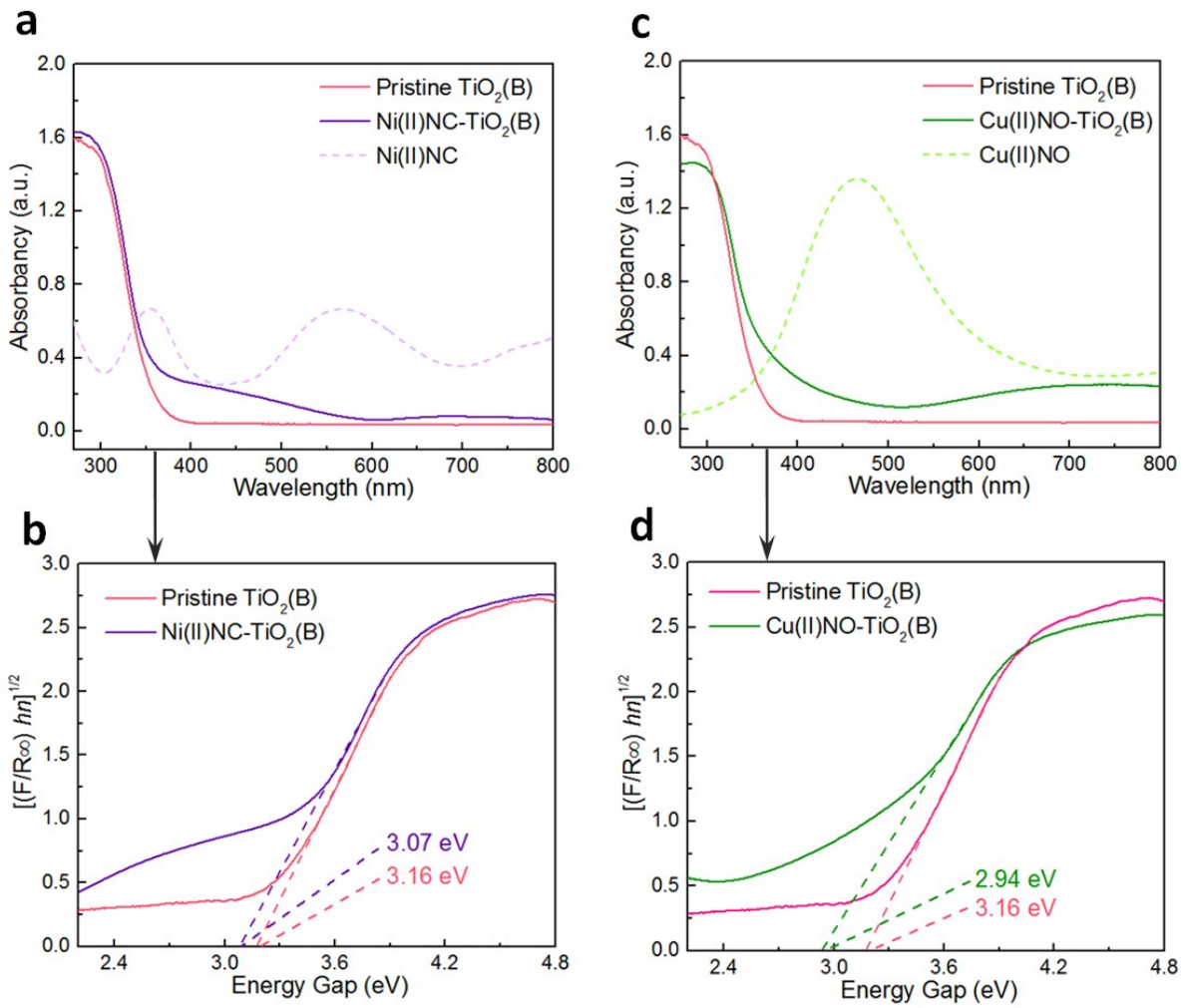

Figure S13. (a) UV-Vis diffuse reflectance spectra of pure TiO_2 (B), Ni(II)NC-TiO_2 (B) and Ni(II)NC and (b) transform of Kubelka-Munk function versus the energy of photon of TiO_2 (B), Ni(II)NC-TiO_2 (B); (c) UV-Vis diffuse reflectance spectra of pure TiO_2 (B), Cu(II)NO-TiO_2 (B) and Cu(II)NO and (d) transform of Kubelka-Munk function versus the energy of photon of TiO_2 (B), Cu(II)NO-TiO_2 (B).

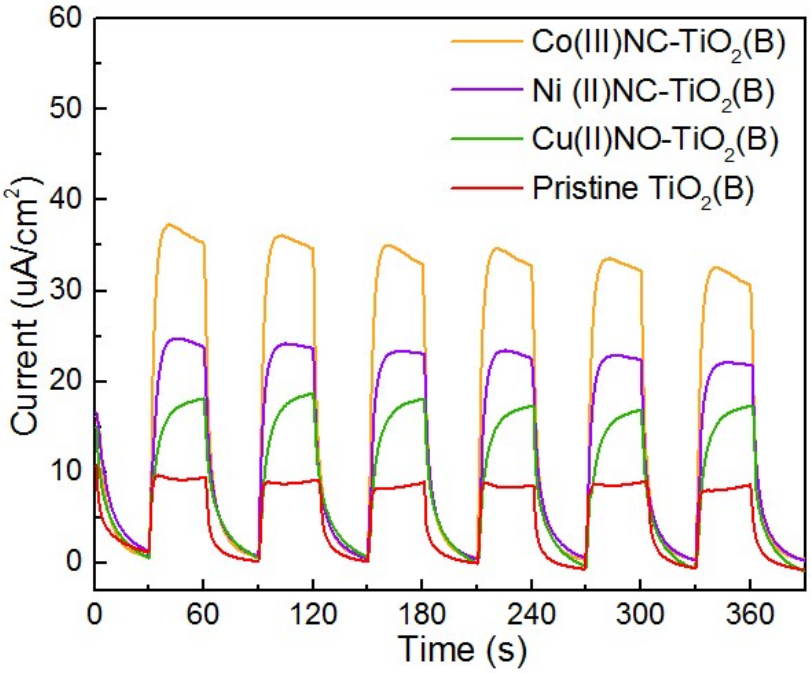

Figure S14. Transient photocurrent responses of Co(Ⅲ)NC/Ni(II)NC/Cu(II)NO-TiO_2 (B) nanosheets using a bias potential of 0.6 V (vs. Ag/AgCl) under on-off cycling irradiation.

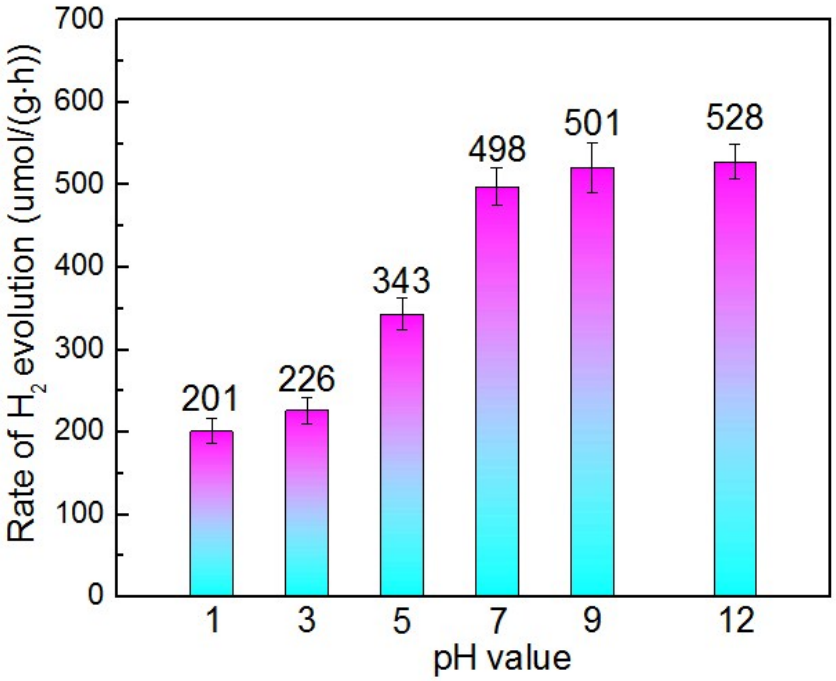

Figure S15. Photocatalytic H_2 evolution activities of Co(III)NC-TiO_2 (B) in aqueous methanol solution with different pH adjusted by dropping $NH_3 \cdot H_2O$ solution.

Table S1 Photocatalytic H_2 evolution performance of TiO_2 materials

Semiconductor	Modification method	Surface specific area	H_2 evolution	Published time	references
Fe_2O_3/TiO_2	Polycrystal mixed growth	28 m^2/g	217.6 μmol/(g•h)	2014	1
Ag/TiO_2	Photodeposition method	15 m^2/g	220 μmol/(g•h)	2015	2
Core–Shell TiO_2	Hydrothermal treatment with hydrofluoric acid	1.6 m^2/g	268.3 μmol/(g•h)	2016	3
$ZnTiO_3/TiO_2$	Hydrothermal treatment of zeolitic imidazolate framework	132 m^2/g	192.5 μmol/(g•h)	2017	4
Branched TiO_2	Alkali-hydrothermal method	205.5 m^2/g	410 μmol/(g•h)	2017	5
Au/TiO_2	Sol immobilization method	---	65 μmol/(g•h)	2018	6
RGO/ TiO_2	Sol–gel electrospinning method	55 m^2/g	149 μmol/(g•h)	2018	7
Plasma TiO_2 (B)	Plasma engraving	515 m^2/g	155 μmol/(g•h)	2018	8
TiO_2 (B)-ZnO	Reflux method	23.3 m^2/g	193μmol/(g•h)	2018	9
$Au/TiO_2–gC_3N_4$	Sol–gel and chemical reduction	75 m^2/g	350 μmol/(g•h)	2018	10
Pt- TiO_2 (B)	Photodeposition method	301 m^2/g	869.4 μmol/(g•h)		**This work**
Co(III)NC-TiO_2 (B)	Electrostatic adsorption	316 m^2/g	497.8 μmol/(g•h)		**This work**
Ni(II)NC-TiO_2 (B)	Electrostatic adsorption	309 m^2/g	431.6 μmol/(g•h)		**This work**
Cu(II)NO-TiO_2 (B)	Electrostatic adsorption	321 m^2/g	364.6 μmol/(g•h)		**This work**

References

1. K. Afroz, M. Moniruddin, N. Bakranov, S. Kudaibergenov and N. Nuraje, *J. Mater. Chem. A*, 2018, DOI: 10.1039/c8ta04165b.
2. Y. Choi, H.-i. Kim, G.-h. Moon, S. Jo and W. Choi, *ACS Catal.*, 2016, **6**, 821-828.
3. Y. Yang, G. Liu, J. T. Irvine and H. M. Cheng, *Adv. Mater.*, 2016, **28**, 5850-5856.
4. H. Tian, S. Wang, C. Zhang, J.-P. Veder, J. Pan, M. Jaroniec, L. Wang and J. Liu, *J. Mater. Chem. A*, 2017, **5**, 11615-11622.
5. G. Yang, L. Wang, S. Peng, J. Wang, D. Ji, W. Yan and S. Ramakrishna, *Small*, 2017, **13**.
6. J. Nie, J. Schneider, F. Sieland, L. Zhou, S. Xia and D. W. Bahnemann, *RSC Adv.*, 2018, **8**, 25881-25887.
7. D. Xu, L. Li, R. He, L. Qi, L. Zhang and B. Cheng, *Appl. Surf. Sci.*, 2018, **434**, 620-625.
8. X. Kong, Y. Xu, Z. Cui, Z. Li, Y. Liang, Z. Gao, S. Zhu and X. Yang, *Appl. Catal. B: Environ.*, 2018, **230**, 11-17.
9. C. Sun, Q. Xu, Y. Xie, Y. Ling and Y. Hou, *J. Mater. Chem. A*, 2018, **6**, 8289-8298.
10. C. Marchal, T. Cottineau, M. G. Méndez-Medrano, C. Colbeau-Justin, V. Caps and V. Keller, *Advanced Energy Mater.*, 2018, **8**, 1702142.